

# AUTOMATIC DETECTION OF FEATURES IN ULTRASOUND IMAGES OF THE EYE

R.Youmaran<sup>1</sup>, P. Dicorato<sup>1</sup>, R. Munger<sup>2</sup>, T.Hall<sup>1</sup>, A. Adler<sup>1</sup>  
<sup>1</sup> School of Information Technology and Engineering (SITE),  
University of Ottawa, Ontario Canada  
<sup>2</sup>University of Ottawa Eye Institute, Ottawa, Ontario, Canada

*Abstract--In closed angled Glaucoma, fluid pressure in the eye increases because of inadequate fluid flow between the iris and the cornea. One important technique to assess patients at risk of glaucoma is to analyze ultrasound images of the eye to detect the structural changes. Currently, these images are analyzed manually. We propose an algorithm to automatically identify clinically important features in the ultrasound image of the eye. The main challenge is stable detection of features in the presence of ultrasound speckle noise; the algorithm addresses this using multiscale analysis and template matching. Tests were performed by comparison of results with eighty images of glaucoma patients and normals against the landmarks identified by a trained technologist. In 5% of cases, the algorithm could not analyze the images; in the remaining cases, features were correctly identified (within 97.5  $\mu$ m) in 97% of images. This work shows promise as a technique to improve the efficiency of clinical interpretation of ultrasound images of the eye.*

## I. INTRODUCTION

Glaucoma is one of the leading causes of blindness. In closed angled Glaucoma, fluid pressure in the eye increases because of inadequate fluid flow between the iris and the cornea. The pressure causes damage and eventually death of nerve fibers responsible for vision [10]. One important technique to assess patients at risk of glaucoma is to analyze ultrasound images of the eye to detect the structural changes that reduce the flow of fluids out of the eye [6]. Usually, sequences of ultrasound images of the eye are analyzed manually; a trained technologist determines anatomical feature locations and measures the relevant clinical parameters. The main features within the eye of clinical interest are: the sclera, a dense, fibrous opaque white outer coat enclosing the eyeball except the part covered by the cornea; the scleral spur, a small triangular region in a meridional section of the sclera tissue with its base along the inner surface of the sclera; the anterior chamber, the region bounded by the posterior surface of the cornea and the central part of the lens; and, the trabecular-iris recess, the apex point between the sclera region and the iris. Manual analysis of eye images is fairly time consuming, and the accuracy of parameter

measurements varies between experts. For this reason, we were motivated to develop an algorithm to automatically analyze eye ultrasound images. We anticipate that this algorithm will reduce the processing time currently taken by the technologist to analyze patient images and extract the clinical parameters of interest. The difficulties in measuring these parameters are associated with noise, poor contrast, poor resolution, and weak edge (boundary) delineation inherently present in ultrasound images [8].

## II. ALGORITHM DESIGN

This section develops an algorithm to automate the measurement of the location of clinically relevant features in ultrasound images of the eye. The proposed algorithm is designed to calculate two clinical parameters, the *open-angle* and *AOD 500*, as shown in Fig. 1 and defined in [5, 6, 9]. In performing this calculation, it must delineate the sclera, and locate the scleral spur, the trabecular-iris recess, and the anterior chamber. The algorithm is structured into three steps, shown in Fig. 2: steps 1 and 2 are executed independently and the result merged into step 3 to complete the feature extraction and resultant calculations.

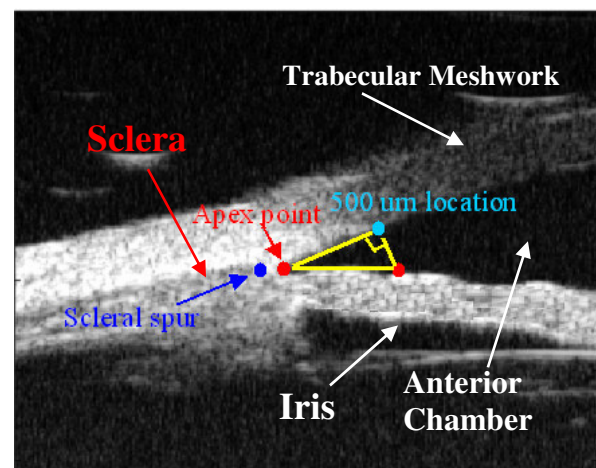


Fig. 1: Clinical features of interest

## A. STEP 1

The goal of this section is to extract from the image the anterior chamber region. The sequences of operations are described in the flowchart (Fig.2). All image operations are based on rectangular pixels of  $19.5 \mu\text{m} \times 19.5 \mu\text{m}$ .

**1.1 Image thresholding:** An intensity threshold, THR, is selected based on a subset of images of the anterior chamber region cropped manually. THR is selected at the tail of the histogram for the anterior chamber region. Once obtained, THR is fixed for all scanned images. Pixels with intensity above THR are set to 255; otherwise, the value is unchanged. The thresholded image is denoted as  $f_{\text{th1}}$ .

**1.2 Non-Linear Edge & Contrast Enhancement:**  $f_{\text{th1}}$  is low pass filtered with a  $9 \times 9$  Gaussian filter with  $N=8$  iterations, using the non-linear edge and contrast enhancement algorithm of [1,2]. The output of this system results in a coarsely enhanced image  $f_{\text{enh1}}$  with reduced noise and high-frequencies content.

**1.3 Image Binarization:** Using the grayscale threshold, THR, the quasi-binary enhanced image ( $f_{\text{enh1}}$ ) pixels are binarized (Fig. 3).



Fig. 3: Coarsely enhanced binary image using the Non-Linear Edge & Contrast Enhancement algorithm

**1.4 Image erosion:** Erosion is applied on the binary image to remove spurious features. A  $5 \times 5$  square-shaped structuring element is used for the erosion process. The resultant image is denoted by " $f_{\text{er1}}$ ".

**1.5 Hole Filling:** small openings (holes) in the trabecular meshwork and the iris are detected and filled. The filled image ' $f_{\text{fill1}}$ ' is later used for correlation with a template image of the anterior chamber (section 1.6).

**1.6 Template Correlation:** The anterior chamber is a large and roughly triangular feature, and can thus be identified using correlation with an appropriate template. In order to compensate for variability in the shape of this region, 3 template regions were chosen from representative image (Fig. 4) of subjects with different degrees of glaucoma.



Fig. 4: Template images used for the correlation process for the detection of the anterior chamber. Each image is of different size and shape to represent the variability of the degree of glaucoma.

The enhanced image is then correlated with each template and the average correlation point  $(x_c, y_c)$  computed from the mean of all maximum correlation points.

**1.7 Anterior Chamber Classification and Segmentation:** Each closed region in " $f_{\text{fill1}}$ " is analyzed to identify the most likely to be the anterior chamber. Classification is based on the geometrical properties: object area, centroid, and major-axis and minor-axis length (using an elliptical model). The following parameters are computed for segmentation of each closed region:

- Center: Defined as the center coordinate of a region
- Distance from maximum correlation point  $(x_c, y_c)$ : Defined as the distance between the calculated center in (a) and the average correlation point  $(x_c, y_c)$  computed in section 1.6.
- Area: Defined as the total number of pixels characterizing a closed region.

The regions that meet the following requirements are to be considered as candidates in the segmentation process.

- Area  $> 50$  pixels; otherwise, the region is considered to be speckle noise.
- The distance between the center of the closed region and  $(x_c, y_c)$  must be minimum; ideally zero.

If more than one region have the same minimum distance  $(x_c, y_c)$ , then the selection is based on the maximum area. Once the anterior chamber is segmented, the upper and lower edge coordinates are extracted. Also, the apex point  $(x_{\text{apex}}, y_{\text{apex}})$  is defined by locating the black pixel that is the most to the left of the anterior chamber as shown in Fig. 1. If no regions are detected, the algorithm terminates since the coordinates of the anterior chamber cannot be calculated.

## B. STEP 2

The goal of this section of the algorithm is to identify the sclera region.

**2.1 Histogram magnification:** A histogram magnification (Fig. 5) is applied to enhance the texture of interest. Threshold values are calculated corresponding to 15% and 85% of the total number of pixels in the histogram.

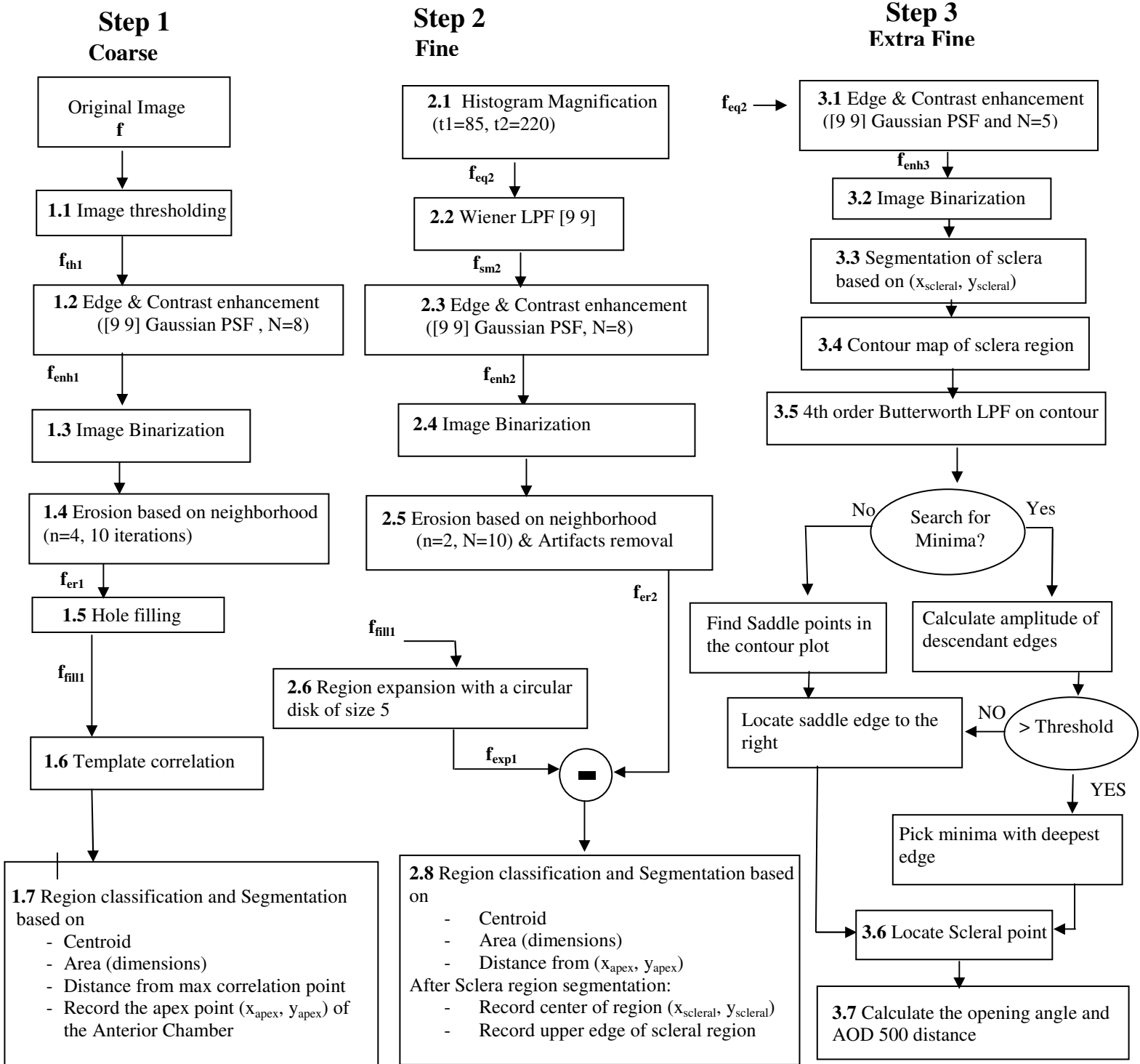


Fig. 2: Flowchart illustrating main algorithmic steps

**2.2 Wiener Filtering:** The image is filtered using the Wiener filter [3, 7] with noise estimates computed using a neighborhood of 9x9 pixels.

**2.3 Non-linear Edge & Contrast Enhancement:** Using the same iterative process with identical parameters as in Section 1.2.

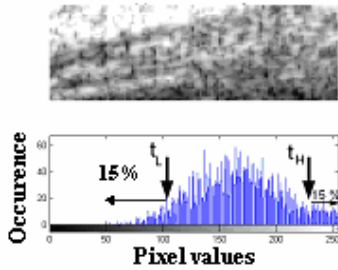


Fig. 5: Cropped Sclera Region & its corresponding histogram. The upper and lower thresholds are depicted on the histogram

**2.4 Image Binarization:** Using the same process and threshold as Section 1.3, to obtain a finely enhanced binary image (Fig. 6).



Fig. 6: Finely enhanced binary image (output of step 2.4). The sclera region (region of interest) is circled

**2.5 Image Erosion:** iterative erosion is repeated for  $n=4$  times to remove artifacts in the enhanced binary images. The classic 3x3 erosion operator is modified in order to preserve weak edges, as follows: the center pixel (located at 0,0) is set to background if and only if both adjacent (horizontal or vertical) pixels are background. The resultant image is denoted by “ $f_{er2}$ ”.

**2.6 Region expansion:** “ $f_{fill1}$ ” is dilated with a circular-shaped structuring element of size 5. This enlarges all regions in the image denoted by “ $f_{exp1}$ ”, which is used for the subtraction process described in the Section 2.7.

**2.7 Region subtraction:** The expanded image (coarsely enhanced) “ $f_{exp1}$ ” is subtracted from the eroded image (finely enhanced) “ $f_{er2}$ ”. This procedure removes all large regions in the image and keeps only the fine details of interest.

**2.8 Sclera region classification and segmentation:**

For segmentation of the sclera region, the following parameters are computed:

- (a) Boundary pixels coordinate: the pixel that is furthest to the right and is located within each of the closed regions ( $x_{right}, y_{right}$ ).
- (b) Distance from the apex point ( $x_{apex}, y_{apex}$ ) of the anterior chamber for each classified region.
- (c) Area in pixels of each region.
- (d) Major axis length of the closed regions.

Regions which meet the following requirements are candidates in the segmentation process.

- i. Area > 50 pixels; otherwise, the region is considered to be speckle noise or too small to be sclera region candidate.
- ii. The distance between ( $x_{right}, y_{right}$ ) and ( $x_{apex}, y_{apex}$ ) is calculated. This distance must be as small as possible since we know that the sclera region is located very close to the apex point of the anterior chamber region.

If multiple regions have the same minimum distance, then the selection is based on the area and the major-axis length, based on observed ultrasound images of the eye. Once the sclera is segmented, its center ( $x_{scleral}, y_{scleral}$ ) as well as its upper edge coordinates are extracted.

**C. STEP 3**

The goal of this section is to improve the robustness of the detection by applying extra fine enhancement to the original image and re-extracting a new sclera region. If the newly extracted scleral spur coordinates correlates with the one previously calculated, then the remaining clinical parameters can be computed; otherwise, the sclera region cannot be segmented, and the algorithm terminates.

**3.1 Non-Linear Edge & Contrast Enhancement:** The enhancement algorithm (Section 2.3) is applied to  $f_{eq2}$  computed in Section 2.1. In order to achieve fine enhancement, fewer iterations ( $N=5$ ) are used, resulting in a significant reduction of the blur. The enhanced image is denoted as “ $f_{enh3}$ ”.

**3.2 Image Binarization:** Same as in Section 1.3.

**3.3 Sclera region Classification and Segmentation:** The approach of section 2.8 is used except an additional parameter is used to account for the distance ( $d_{c-sc}$ ) between the center of each detected candidate region and ( $x_{scleral}, y_{scleral}$ ). A region is classified as the best sclera

candidate if it passes all the requirements of section 2.8 and has the smallest  $d_{c-sc}$ .

**3.4 Sclera Contour Mapping:** Once the sclera has been identified (Fig. 7a), the scleral spur is located based on signal processing on the outline of the top boundary of the extracted sclera region. This outline is determined by scanning the image vertically and determining the uppermost location of the pixels on the scleral image (Fig. 7).

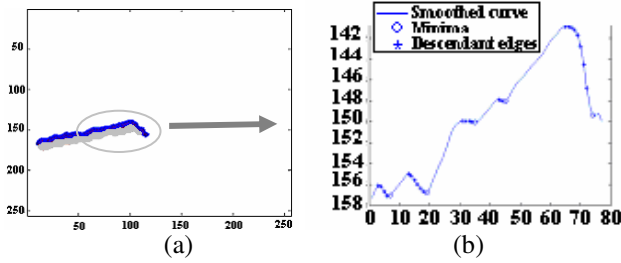


Fig. 7: (a) sclera region with outline mapped onto image, (b) Plot of cropped desired outline (right half section of the sclera outline) showing minima and descendant edges sample points on the smoothed sclera contour. The x-y axes are the spatial coordinates of the image. The x-axis of the cropped outline in (b) represents the number of sample points in the image.

**3.5 Sclera Contour Smoothing Filter Design:** A non-recursive 4<sup>th</sup> order Butterworth smoothing filter, with normalized cutoff frequency ( $\Omega_c$ ) of 0.45, is used to remove outliers and abrupt variations (fluctuations) in the outline that may result from poor resolution and image noise. The filtered data set is defined as  $F_{fit}(x)$ . The value of the normalized cutoff frequency was manually tuned to provide a compromise in terms shape fidelity to the shape and rejection of unwanted saddle points. Since we know that scleral spur is located to the right of the sclera region, only the right-half side of the data points on the sclera contour is searched. This truncation of the size of the detected outline reduces the search time. This new array of data is denoted as “ $F_{trunc}(x)$ ”.

**3.6 Scleral Spur Detection:** The scleral spur is detected from  $F_{trunc}(x)$ , as shown in Fig. 7b, based on the following steps:

- (1) A gradient operator is applied on  $F_{trunc}(x)$ .
- (2) All minima coordinates as well as the points along the descendent edge prior to each local minimum are computed.
- (3) If no minima are detected, all points with zero gradient are located and defined as saddle edges.

Identification/detection of the scleral spur occurs when one of the following occurs:

- (4) One local minimum: This point then becomes the scleral spur coordinate.

- (5) Multiple minima: All points along the descendant edges (computed in (2)) are used in order to calculate the magnitude of each edge ( $\Delta_{edge}$ ) prior to a minimum. For each descendent edge found within the outline  $F_{trunc}(x)$ ,  $\Delta_{edge}$  is computed as the difference between the maximum pixel value and the minimum pixel value along that edge. The descendant edge with the largest  $\Delta_{edge}$  symbolizing the deepest dip is chosen as the scleral spur coordinate.

- (6) No minima: The points computed in (3) (saddle edges) represent possible locations of the scleral spur since no minima are present on the sclera contour. Knowing *a priori* that the scleral spur occurs to the right side of the contour, the saddle edge located most to the right of the 1-D outline is selected as the scleral spur coordinate.

The scleral spur coordinate is denoted as  $(x_s, y_s)$ .

**3.7 Determination of Measured Parameters for Glaucoma:** This section describes calculation of: (1) open-angle; and (2) angle-open distance (AOD), as shown in Fig. 1. These parameters require the location of the apex point (Fig. 1) previously computed in section 1.7. This location will be used to define the angle.

**AOD 500 & Open-Angle Calculation:** The AOD 500 is measured along an orthogonal projection from the trabecular meshwork to the iris [5, 6], as illustrated in Fig. 1. Its calculation requires the computation of: 1) the contour along the upper half of the anterior chamber from the scleral spur to the upper vertex, 2) the contour from the scleral spur along the iris on the lower anterior chamber to the lower vertex, and 3) the location 500  $\mu\text{m}$  from the scleral spur along the upper contour of the anterior chamber. If the 500  $\mu\text{m}$  coordinate location appears to the left of the  $(x_{apex}, y_{apex})$  point, then the open-angle is 0°. Otherwise a positive angle can be calculated.

### III. RESULTS

Ultrasound images were obtained from patients at the University of Ottawa Eye Institute using the Ultrasound Biomicroscope (UBM) System Model 840 (Zeiss-Humphrey), using the protocol described in [4]. The images are then stored on the local hard disk in PCX format. As described in [10], UBM measurements are performed with patient in a supine position with the eye open.

The technologist obtains high-gloss prints from the UBM machine, manually identifies the location of the clinical features. The AOD 500 is then calculated with the use of a ruler, and the open-angle is measured with a protractor centered at the apex point of the anterior chamber [6]. Using the algorithm described here, 80 images were processed on a 2.4 GHz Intel Pentium III processor with

512 MB of SDRAM. The algorithm was implemented in Matlab and the execution time for one image is 32 seconds.

In Section 1.1, a threshold (THR) of 50 was used. In step 2.1, the lower and upper thresholds are selected as 85 and 220, respectively. Fig. 1 illustrates all calculated clinical features of interest using this algorithm. By treating the technologist identified parameters as gold standards, we estimated the detection position (offset) error of the algorithm. The offset error distributions are shown in Fig. 8. Overall, the average offset error was 5 pixels in the vertical and 7 pixels in the horizontal direction.

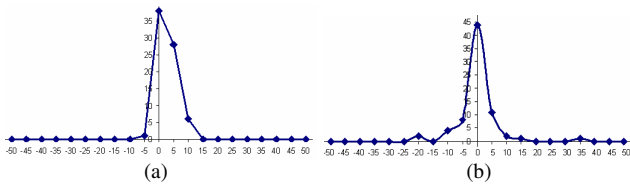


Fig. 8: Offset pixel error distribution in the (a) horizontal direction (b) vertical direction. The x and y axis represent the pixel offset error and occurrences, respectively.

Three possible outcomes can be generated by the developed algorithm. If the algorithm fails to segment the regions of interest or cannot process a specific image, the clinical parameters are not computed (outcome 1). Otherwise, clinical parameters are computed. If the calculated parameters differ from those measured by the technologist within 97.5  $\mu\text{m}$  (5 pixels), the output is considered a success (outcome 2). Otherwise, the offset error is greater than 97.5  $\mu\text{m}$  (5 pixels) in either direction, and the algorithm output is a failure (outcome 3).

Based on the outcomes described above, in 5% of cases, the algorithm could not analyze the images (outcome 1). In the remaining cases, features were correctly identified in 97% of images (outcome 2). Thus, 3% of images presented inaccurate estimates (outcome 3) of the clinical parameters, with 351  $\mu\text{m}$  (18 pixels) offset error average.

#### IV. CONCLUSION

This paper proposes an algorithm to automatically identify clinical features in ultrasound images of the eye. The algorithm computes the AOD 500 and the open-angle parameters used to measure the presence and severity of glaucoma. Overall, the algorithm predictions are very similar to the trained technologist's observation with a small pixel offset error in both the horizontal and vertical directions. The difficulties encountered in measuring clinical parameters are associated with speckle noise; poor contrast, poor resolution, and weak edge delineation present in the processed ultrasound images. These issues

introduced inaccuracy in locating the scleral spur and variability in the measurement of the clinical parameters. The algorithm was designed with a goal of robustness through the use of two-stage (coarse and fine) level enhancement on the original image, and by validation of the proper segmentation of the sclera at each step. We believe that the accuracy of the algorithm can be further improved by adjusting the saddle and minima locator algorithm described in Section 3.6. Overall, the benefits of this work is the ability of algorithm to improve the processing time for each patient's ultrasound image, leading to an increase in efficiency and a reduction of cost.

#### REFERENCES

- [1] Deng G., Cahill L.W., Image Enhancement Using the Log-ratio Approach, *Signals Systems and Computers*, Vol. 1, pp. 198-202, Nov1994
- [2] Deng G., Cahill L.W., Multiscale image enhancement using the logarithmic image processing model, *Electronics Letters*, Vol.29, No.3, pp. 803-804, Apr1993
- [3] J.S. Lim, Two-dimensional Signal and Image processing, Englewoods Cliffs, NJ: Prentice-Hall, pp. 536-540, 1990
- [4] Daneshvar H., Brownstein S., Mintsoulis G., Chialant D., Punja K., Damji KF., Epithelial ingrowth following penetrating keratoplasty:A Clinical, Ultrasound Biomicroscopic and Histopathological Correlation, *Canadian Journal of Ophthalmology*, Vol. 35, No.4, pp. 222-224, Jun 2000
- [5] Nishijima K., Takahashi K., Yamakawa R., Ultrasound Biomicroscopy of the Anterior Segment after Congenital Cataract Surgery, *American Journal of Ophthalmology*, Vol.130, No.4, Oct2000
- [6] Pavlin C.J., Harasiewicz K., Sherar M.D., Foster F.S., Clinical Use of Ultrasound Biomicroscopy, *Ophthalmology*, Vol. 98, No.3, Mar1991
- [7] Polesel, A.; Ramponi, G.; Mathews, V.J., Adaptive unsharp masking for contrast enhancement, Image Processing, 1997 *Proceedings, International Conference on*, Vol.1, No.26, pp. 267 – 270, Oct1997
- [8] Pathak. S. D., Chalana, V., Haynor, D. R., and Kim, Y., Edge-Guided Boundary Delineation in Prostate Ultrasound Images, *IEEE Transactions on Medical Imaging*, Vol.19, No.12, pp. 1211-1219, Dec2000
- [9] American Academy of Ophthalmology, Preferred practice pattern of primary open angle glaucoma, San Francisco: American Academy of Ophthalmology, 1996.
- [10] Bhatt, Deepak, Ultrasound Biomicroscopy, *Journal of the Bombay Ophthalmologists Association*, Vol.12, No.1, Jan2002